Structure of Fe_3Si/GaAs(001) epitaxial films from x-ray crystal truncation rods

Vladimir M. Kaganer, Bernd Jenichen, Roman Shayduk, and Wolfgang Braun
Paul-Drude-Institut für Festkörperelektronik, Hausvogteiplatz 5-7, D-10117 Berlin, Germany
(Received 21 November 2007; published 19 March 2008)

Thin (10–15 nm thick) Fe_3Si films are grown on GaAs(001) by molecular beam epitaxy and studied *in situ* by grazing incidence x-ray diffraction. We find two interfacial structures in different samples, with the first atomic layer of Fe_3Si consisting of either iron atoms only or both Fe and Si atoms. In both cases, the top atomic layer at the surface contains both Fe and Si atoms. The films are fully ordered, except 1 or 2 monolayers at the surface, where Fe and Si atoms within one and the same atomic layer are intermixed.

DOI: 10.1103/PhysRevB.77.125325 PACS number(s): 68.35.−p, 61.05.cp, 68.35.Ct

I. INTRODUCTION

Novel electronic and spintronic device concepts require various combinations of metals, semiconductors, magnetic materials, insulators, etc., with highly perfect interfaces. Materials with different crystal structures and bonding can be grown epitaxially on each other if their lattices are appropriately matched.[1] X-ray diffraction is a powerful tool to study both the structure of an epitaxial film and its arrangement on a substrate, thanks to the interference between waves scattered by the film and the substrate.

Fe_3Si epitaxial films on a GaAs substrate, studied in the present work, are a combination of a ferromagnetic film, with Curie temperature well above room temperature, and a semiconductor. Such a system can be used to inject a spin-oriented electrical current into the semiconductor.[2] An ideal lattice match is achieved by varying the Fe and Si deposition fluxes, close to the stoichiometric composition.[3] The stoichiometric films possess the smallest sheet resistance.[4] A perfectly coherent dislocation-free interface is observed by transmission electron microscopy.[5,6]

A thin crystalline film is a planar object with the scattering pattern consisting of lines [called crystal truncation rods (CTRs)] normal to the interface. The intensity distribution along a CTR results from the interference of the waves scattered by both crystal lattices and hence is highly sensitive to the relative positions of the atoms in crystals. The sensitivity of the CTR scattering to interface structures was first demonstrated by Robinson *et al.*[7,8] in CTR studies of $Si(111)/SiO_2$ and $NiSi_2$ interfaces. CTR measurements have since been used to study interfacial structures of various lattice matching epitaxial systems, such as $CaF_2/Si(111)$,[9–12] $CaSrF_2/GaAs(111)$,[13,14] Ge δ layers on Si(001),[15–17] Pd/MgO(001),[18] and several semiconductor heterostructures.[19–21] Still, x-ray diffraction is much more rarely applied to study interfaces, as compared to surfaces.

Epitaxial films with thicknesses up to several tens of monolayers, the subject of our study, lie in between two well established fields of research. On one end, crystalline surfaces are commonly analyzed in the kinematical (single scattering) approximation.[22,23] On the other end, thicker films and multilayers are studied with dynamical diffraction theory.[24] In surface structure analysis, the regions of strong scattering close to the bulk Bragg reflections, where dynamical calculations are mandatory, are excluded from the analysis. The measured intensity is scaled to the calculated one by using an arbitrary fit parameter. On the other hand, dynamical calculations are very accurate at the Bragg peak but restricted to the close vicinity of the peak, since the two-beam dynamical theory loses its applicability away from the Bragg peak. We have used dynamical calculations to characterize the order in the Fe_3Si/GaAs(001) films.[25] The films were several times thicker, compared to the ones used in the present study, and the vicinity of the Bragg peaks contained all necessary information.

The problem of a dynamical calculation of the diffracted intensity in a wide wave vector range has been the subject of a number of investigations.[26–35] Recently, we have shown[36] that the dynamical calculation can be extended to the whole CTR by summing up the amplitudes of the diffracted waves of the two-beam diffraction problems for all Bragg reflections along the CTR. Dynamical and kinematical scattering intensities quantitatively agree everywhere except in the vicinity of the Bragg peaks, where the kinematical intensity diverges. The dynamical calculation gives, within the Darwin width, a reflectivity close to 1 (and somewhat smaller than 1), which provides an absolute scale for the measured intensity. The absolute intensity is especially important if the structure factors of the film are not known in advance. Fe_3Si is an example: if the long-range order of the Fe and Si sublattices is disturbed, Fe and Si atoms intermix producing antisite defects, and the structure factors of the superstructure reflections decrease or may even vanish. The dynamical Bragg reflections, independent of the long-range order in the film, provide a reference to obtain the structure factors of a partially ordered film.

By comparing the measured CTRs with the calculated ones, we find that the Fe_3Si lattice takes two out of possible four high-symmetry positions with respect to the GaAs lattice. The first Fe_3Si atomic layer at the interface contains only Fe atoms in one case and both Fe and Si atoms in the other. These two epitaxial positions are realized in different samples. We find that the Fe_3Si film exhibits full long-range order in the Fe and Si sublattices, except for atomic layers immediately adjacent to either the surface or the interface, where disorder is observed. The fits imply a relaxation of 0.2 Å of the Fe_3Si film toward the substrate.

II. EXPERIMENT

Fe_3Si films were grown by molecular beam epitaxy (MBE) on GaAs(001) substrates in an MBE chamber inside

the diffractometer at the wiggler beamline U125/2 KMC[37] at the storage ring BESSY in Berlin. A double crystal Si(111) monochromator was used. The energy of the radiation was 10 keV and the incidence angle was 0.3°. The acceptance angle of the detector was 0.1° both perpendicular and parallel to the surface.

GaAs(001) templates were prepared in a separate III-V growth chamber using standard GaAs growth techniques. The sample was then capped by As and transferred into the system at BESSY for the Fe_3Si deposition by means of an ultrahigh vacuum shuttle. The As cap was removed by annealing the sample in the preparation chamber at a temperature of 350 °C before transferring it into the growth chamber. Then, the Fe_3Si layers were grown on the As-rich $c(4\times4)$ reconstructed GaAs surface at different substrate temperatures near 200 °C, similar to the procedure described in Ref. 3. To obtain higher purity and a more stable cell operation, we stayed below the melting point with the Si source. This, together with the relatively large source-sample distance in our chamber, results in a fairly low growth rate of 3 ML (monolayers)/h that would probably not be used for device fabrication. For the *in situ* measurements, however, such a low growth rate allows us to study the growth process *in vivo* with good time resolution.

We define a monolayer as 1 ML$=0.5a\cong0.28$ nm, where a is the lattice parameter, based on the observation of the x-ray intensity oscillations during layer-by-layer growth of Fe_3Si.[38] The Si and Fe cell temperatures were tuned in order to obtain a perfect lattice match of the films, as monitored by the position of the Fe_3Si layer diffraction peak with respect to the GaAs peak. We obtained optimum temperatures of 1239 and 1370 °C for the Fe and the Si cells, respectively.

The measurements were performed along straight lines in reciprocal space under SPEC™ software control. The end points of a CTR were adjusted prior to the CTR measurement. The accuracy of such scans was verified by comparing equivalent reflections (see Fig. 6 below). More elaborate CTR measurements by making sample rotations about the sample normal and collecting integrated intensities would be too time consuming for our measurements with intensity oscillations along each CTR.

III. CALCULATION OF CRYSTAL TRUNCATION RODS

Surface structure analysis is commonly performed in the kinematical (single scattering) approximation.[22,23] The amplitude of the electromagnetic wave scattered by a crystalline film on a substrate reads

$$E^{\mathrm{kin}}=\frac{\lambda r_e}{ia^2\sin\Phi_{\mathrm{out}}}\left[\frac{F_s}{1-\exp(2\pi iLN)}+F_f\frac{1-\exp(2\pi iLN)}{1-\exp(2\pi iL)}\right]. \tag{1}$$

Here, λ is the wavelength, r_e is the classical radius of the electron, a is the lattice spacing, Φ_{out} is the angle between the scattered wave and the crystal surface, $L=aQ_z/2\pi$ is the continuous reciprocal space coordinate along the CTR, Q_z is the momentum transfer component along surface normal (chosen as the z axis), N is the film thickness measured in number of unit cells, and F_s and F_f are the structure factors of the substrate and the film, respectively. They are calculated at the point hkL in reciprocal space, where h and k are the in-plane Miller indices defining the CTR. A generalization of Eq. (1) to a multilayer structure is straightforward: the jth layer contributes to the sum with an additional phase factor $\exp(2\pi iLt_j)$, where t_j is the total thickness of all layers located above it.

The kinematical approximation loses its applicability in the cases of grazing incidence or grazing exit, when the angle of either the incident or the exiting wave to the surface is comparable with the critical angle for total external reflection. Since our experiments are performed with an incidence angle $\Phi_{\mathrm{in}}=0.3°$, just barely above the critical angle $\alpha_c=0.24°$, we extend the kinematical approximation by the distorted-wave Born approximation (DWBA).[36] In this approximation, the incident and scattered plane waves in vacuum are replaced by the waves in the medium having the same mean polarizability as in the system under investigation. Two sets of crystal waves are involved, corresponding to vacuum waves incident on the surface under the incidence angles Φ_{in} and Φ_{out}, respectively. The solution of each problem in the medium consists of two plane waves with the amplitudes D_n $(n=1,2)$, corresponding to the transmitted and the specularly reflected waves in vacuum. Our calculations on $Fe_3Si/GaAs(001)$ films show that the quantitative agreement between DWBA and the dynamical calculation described below can be reached when the difference in mean polarizabilities between the substrate and film materials is taken into account, so that the amplitudes D_{sn} and D_{fn} in the substrate and in the film are distinguished. Then, the kinematical solution [Eq. (1)] is replaced by

$$E^{\mathrm{DWBA}}=\frac{\lambda r_e}{ia^2\sin\Phi_{\mathrm{out}}}\sum_{m,n=1,2}\left[\frac{D_{sm}^{\mathrm{in}}D_{sn}^{\mathrm{out}}F_s}{1-\exp(2\pi iL_{smn})}+D_{fm}^{\mathrm{in}}D_{fn}^{\mathrm{out}}F_f\frac{1-\exp(2\pi iL_{fmn}N)}{1-\exp(2\pi iL_{fmn})}\right]. \tag{2}$$

The superscripts "in" and "out" distinguish the two sets of crystal waves. The parameters $L_{mn}=(a/\lambda)(u_m^{\mathrm{in}}+u_n^{\mathrm{out}})$ for the substrate and the film are z components of the wave vectors in the media, $u_n=k_{nz}/\kappa$. Here, $\mathbf{k}_n$ are the wave vectors of the waves inside the medium (substrate or film, respectively) and $\kappa=2\pi/\lambda$. Complex parameters L_{mn} substitute the real parameter L in Eq. (1).

Close to a Bragg peak, the kinematical and DWBA solutions diverge. The correct scattering intensities can be obtained in the vicinity of each Bragg reflection hkl (where h, k, and l are the integer Miller indices) by solving the corresponding two-beam dynamical diffraction problem. The amplitude of the scattered wave E_{hkl}^{dyn} is a function of the deviation $L-l$ from the Bragg point. For large deviations, the diffraction problem becomes multibeam. However, there is no need to solve the full multibeam problem: to first order in the polarizability χ, it can be split into a sum of two-beam problems. The dynamical scattering amplitude along a CTR then becomes the sum of the solutions of the two-beam amplitudes for all Bragg reflections along this CTR,[36]

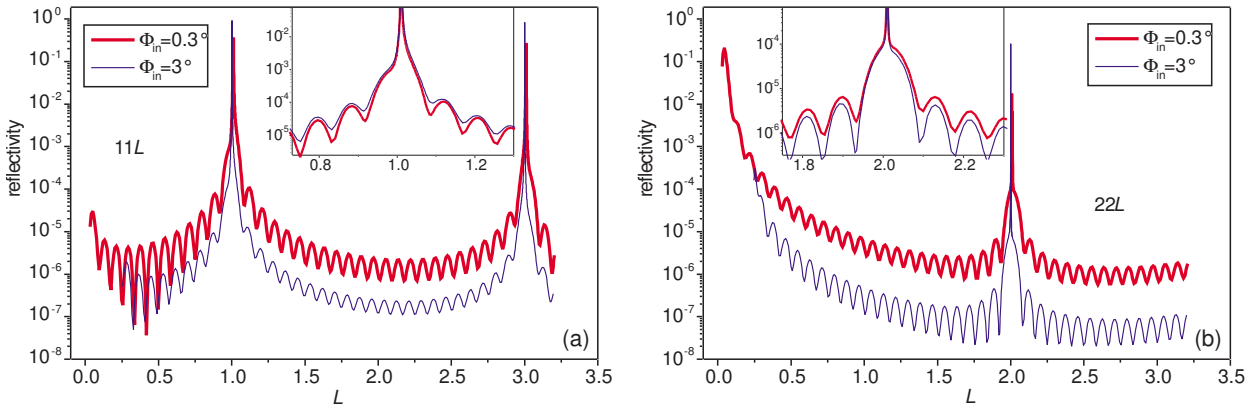

FIG. 1. (Color online) Calculated crystal truncation rods 11L and 22L from a Fe_3Si epitaxial film on GaAs(001). The film thickness is 24 ML (13.6 nm). Reflectivity curves are obtained at a grazing incidence angle $\Phi_{in}=0.3°$ (thick red lines) and nongrazing incidence angle $\Phi_{in}=3°$ (thin blue lines). The insets show the vicinities of the Bragg reflections, with the nongrazing curves arbitrarily scaled to the grazing incidence ones. The misfit between Fe_3Si and GaAs lattices is set to zero.

$$E^{\mathrm{dyn}}(hkL) = \sum_l E^{\mathrm{dyn}}_{hkl}. \tag{3}$$

Since the x-ray polarizability χ is typically of the order of 10^{-5}, there is no practical need for a multibeam calculation that would provide a correction to the intensity of the order of χ^2. Moreover, dynamical theory, in either its two-beam or multibeam formulation, inaccurately treats the surface layer,[36] which gives rise to an error around $10^{-7}-10^{-8}$ of the peak intensity. The error originates from the Fourier expansion of the electron density in a periodic medium that is used in dynamical theory. The electron density is truncated at a mathematically flat surface, thus cutting off parts of the electron density, which belong to the topmost atoms. Kinematical theory considers electron densities of individual atoms and therefore is more accurate for such low intensities.[36]

Figure 1 presents two calculated CTRs, 11L and 22L, from a 24 ML (13.6 nm) thick Fe_3Si layer on GaAs(001). Instead of the scattered wave intensity $I=|E|^2$, the reflectivity $R=I \sin \Phi_{out}/\sin \Phi_{in}$ is plotted. The reflectivity is always less than 1 and close to 1 at the allowed Bragg reflections. The DWBA calculation of Eq. (2) and the dynamical calculation of Eq. (3) with 16 reflections included in the sum give coinciding reflectivites—the difference between the curves is less than the thickness of the lines in the figure. The exception is the vicinity of the Bragg peaks, where the DWBA intensity diverges (not shown in the figure). Practically, we use the dynamical formula if the reflectivity R is larger than 10^{-3} and DWBA otherwise, since the DWBA calculation is faster.

Thick (red) lines in Fig. 1 are calculated for $\Phi_{in}=0.3°$, which is the incidence angle used in our experiments. For comparison, thin (blue) lines show the reflectivity at an incidence angle $\Phi_{in}=3°$. At such a large incidence angle, the kinematical formula [Eq. (1)] is valid. Dynamical intensities of the Bragg peaks are larger for the larger incidence angle. However, between the Bragg peaks, the reflectivity at the grazing incidence angle of 0.3° is an order of magnitude larger, thus validating the use of grazing incidence diffraction to study thin Fe_3Si films in the present work.

The two curves calculated for grazing and nongrazing incidence diffractions can be used to evaluate the DWBA corrections to the kinematical formula. In surface structure studies, the regions of large intensity close to the Bragg peak are excluded from consideration, and the remaining curve is arbitrarily scaled in intensity to fit the experimental curve. Such a procedure gets rid of the order of magnitude offset between the curves in Fig. 1. However, the difference in the curve shapes is not removed. The insets of Fig. 1 enlarge the vicinity of the Bragg peaks 111 and 222, with the kinematical curve (blue thin line) manually scaled to the DWBA calculation for grazing incidence diffraction. The differences in the oscillation amplitudes are evident. The amplitude of thickness oscillations is larger in the grazing incidence case for CTR 11L but smaller for 22L. This difference would be missed if kinematical calculations were performed for grazing incidence diffraction. These amplitude variations notably depend on the film thickness. They are minor for a bare substrate or films of a few monolayers thick (thus justifying the use of the kinematical approximation in surface structure analysis even at grazing incidence), but become remarkable for films with a thickness of several tens of monolayers.

IV. RESULTS

Crystalline Fe_3Si has the $D0_3$ structure (space group $Fm\bar{3}m$). Its cubic unit cell consists of layers occupied either by only Fe or by Fe and Si atoms in an alternating regular arrangement (see Fig. 2). The lattice spacing of Fe_3Si is very close to that of GaAs: the mismatch found by fitting the CTRs in the present study is 0.3%. Four high-symmetry variants to place the Fe_3Si crystal lattice on GaAs are shown in Fig. 2. The first atomic layer of Fe_3Si adjacent to the top As layer of GaAs can contain either Fe and Si atoms (variant A) or only Fe atoms (variant B). Two further variants (C and D) are obtained by an $a/2$ translation of the Fe_3Si unit cell in the [100] direction.

Since x-ray diffraction is highly sensitive to the interference between the waves scattered by the substrate lattice and

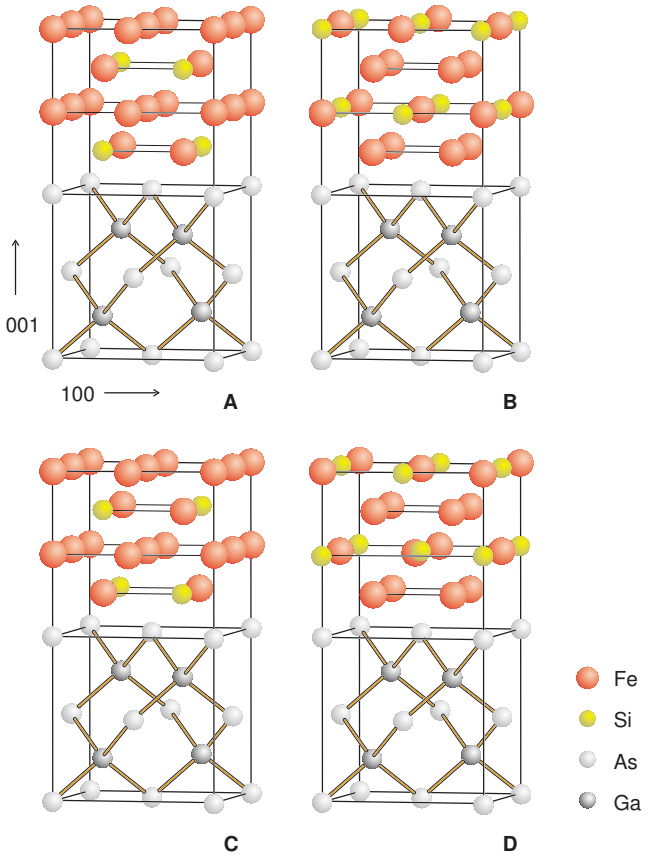

FIG. 2. (Color online) Four high-symmetry variants of placing the Fe_3Si unit cell on GaAs(001).

the ones scattered by the film lattice, the CTRs calculated for these four arrangements of the film on the substrate have qualitatively different shapes. Figure 3 compares calculated CTRs 11*L* for variants A–D with the CTRs measured on two different samples. We find that two, out of possible four, interfacial arrangements are observed in our experiments.

The calculated curves in Fig. 3 differ in the position of the layer peak and the respective positions of the thickness oscillations. A curve calculated for one of variants A–D can be transformed to another one by imposing a mismatch of about 2%. If only one CTR is measured on a given sample, an erroneous determination of both the interfacial structure and the mismatch can therefore result. However, by measuring and simulating a number of CTRs, as shown in Fig. 6 below, we can exclude such misinterpretation. We find that the curves in the vicinity of 002 and 222 reflections are very sensitive to the mismatch. A fit of these CTRs unambiguously determines a mismatch of 0.3%–0.4% in all samples. Each experimental curve is scaled to the calculated one by requiring that the integrated intensity of the Bragg peak is the same. For the top curve in Fig. 3 (variant A), such a scaling of the substrate peak results in a complete agreement of the measured and calculated CTRs. To obtain an agreement for the second curve (variant B), the measured intensities needed to be multiplied by a factor of 1.5.

From six samples that we have grown and investigated, the lattice placement variants A and B are found in three samples each. We discuss in detail the measurements on two

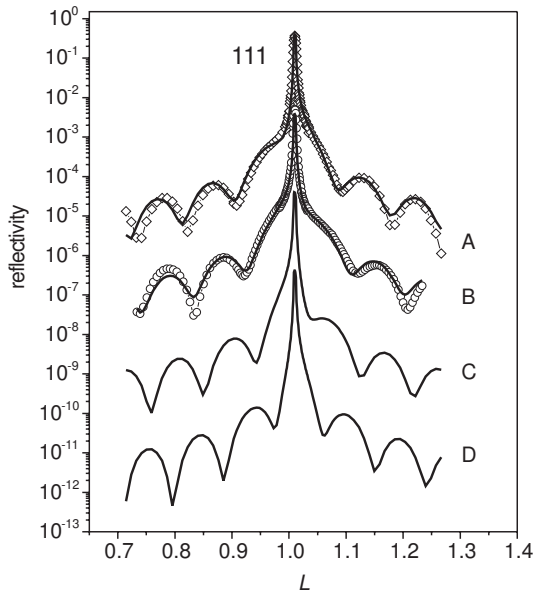

FIG. 3. Crystal truncation rods 11*L* calculated for the interfacial variants A–D in Fig. 2 (full lines) and experimental data from two samples, A and B (open symbols). Two other variants, C and D, are not realized in our experiment. The curves are shifted vertically by two decades for clarity.

samples, demonstrating variants A and B, respectively. We refer to these samples as A and B samples, thus indicating the structure relevant to each of them. Other samples show very similar CTRs of either one or the other variant. Variants A and B are clearly distinguished, since they reveal the broad layer peak shifted with respect to the narrow substrate peak to left or to right, respectively. Variants C and D give rise to more narrow layer peaks and are also clearly distinguishable. The presence of domains of different variants in one sample would smear the difference between the variants. For example, the presence of A and B domains in equal amounts was to produce a symmetric layer peak centered at the substrate peak. Since the two experimental curves in Fig. 3 are notably different and agree well with the corresponding calculated curves, we conclude that domains of different interface variants are not mixed in a single sample. The samples were grown under nominally the same conditions, and we cannot relate the appearance of an interfacial variant to the choice of growth parameters. The probably least controlled procedure is the As desorption from the substrate after its transport to the beamline system. Thus, the type of the interfacial arrangement may be related to the residual arsenic on the substrate surface. In both interfacial structures A and B, the silicon atoms in the first FeSi atomic layer are located in between the top chain of Ga-As atoms of the GaAs substrate. In the two other variants, C and D, which are not found in the experiments, the Si atoms are located above these chains.

The 111 reflection investigated in Fig. 3 is sensitive to the long-range order within Fe and Si sublattices.[25] The order is described by 2 order parameters, α and β. The fraction of Si atoms exchanging with Fe atoms within one and the same atomic layer in Fig. 2 is denoted by $\beta \leqslant 0.5$, while the fraction of Si exchanging with Fe atoms in each of the two sublattices of the iron-only layer is given by $\alpha \leqslant 0.25$. The

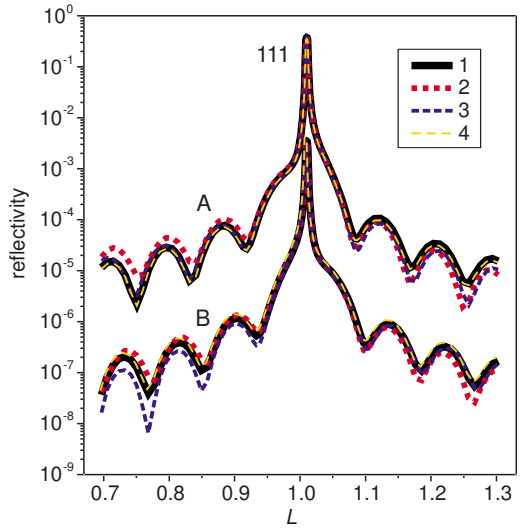

FIG. 4. (Color online) Calculated CTRs for different interfacial and surface structures: (1) an ideal Fe_3Si film on GaAs substrate, (2) Fe atoms are added in between As atoms in the top As layer of GaAs, (3) Si atoms in the first Fe_3Si layer at the interface are replaced by As atoms, and (4) a 2 ML thick layer of FeSi with CsCl structure is added at the surface. Variants A and B of the relative positions of the film and the substrate are shown. The curves are shifted vertically by two decades for clarity.

structure factor of the 111 reflection of a partially disordered Fe_3Si crystal (as well as all other reflections with the odd Miller indices) is $F=4i(1-2\alpha-\beta)(f_{Si}-f_{Fe})$, where f_{Si} and f_{Fe} are the atomic scattering factors of the respective elements. Disorder reduces the structure factor of the Fe_3Si and suppresses the thickness oscillations on CTRs. The agreement of the measured CTRs with the ones calculated for the ordered Fe_3Si crystal in Fig. 3 points to a practically perfect long-range order in our Fe_3Si epitaxial films.

In Fig. 2, we show possible relative positions of the GaAs and Fe_3Si bulk unit cells and do not attempt to model an atomic structure of the interface. The thickness of the interface ($\approx$1 ML) is small compared to the layer thickness (more than 20 ML). As a result, diffraction curves A–D in Fig. 3 are fairly sensitive to the relative positions of the crystal lattices of the layer and the substrate but less sensitive to the details of the atomic structure of the interface. Figure 4 compares diffraction curves calculated for different interfacial and surface structures. Curve 1 presents an ideal lattice matched Fe_3Si film of 24 ML thickness for lattice placements A and B. For variant A, the top Fe atomic layer is removed, as is described below in the detailed modeling of sample A. Hence, the Fe_3Si layer ends by a FeSi atomic layer on the surface in both cases A and B. Curve 2 is calculated for the same model with extra Fe atoms added in between As atoms in the top As layer of the substrate. Curve 3 is obtained by replacing Si atoms in the first monolayer at the interface by As atoms. Curve 4 models the silicon rich surface of Fe_3Si by adding a one unit cell (2 ML thick) layer of FeSi crystal with the CsCl structure.[40–44] Modifications of the surface or the interface give rise to relatively small, albeit visible, differences in the diffraction curves. We have also tried several other plausible models but did not reach a substantial improvement in the agreement between the measured and the calculated diffraction curves. Thus, we restrict ourselves to the bulk structures of the substrate and the layer shown in Fig. 2 and do not consider details of the atomic arrangement of the surface and the interface. The agreement between the experiment and the calculations in Figs. 3, 5, and 6 is good, but not perfect, which points to a more complicated atomic structure of the surface and interface than assumed in the present paper. A detailed analysis of these structures is out of the scope of the present paper.

Figure 5 presents the CTRs 11L and 22L of sample A measured in large L ranges. The measured intensities were corrected using the common polarization, Lorentz, rod interception, and active area corrections.[39] Apart from these, we make a correction to the resolution change along the CTR, since we measure only the peak intensity along the CTR and do not perform rocking scans. Instead, we take into account that the width of the rocking scans, measured on a bare substrate, increases proportional to L, except for small L where it approaches a constant value.[37]

The scale factor for the experimental intensity is obtained by the requirement that the integrated intensity of the substrate peak 111 or 222, respectively, is the same as the calculated one. A crucial check of such scaling is the 22L rod,

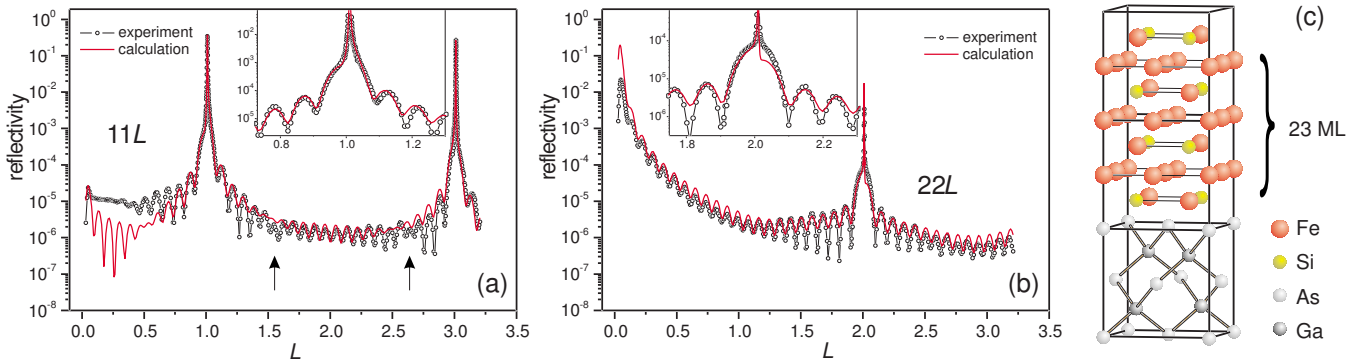

FIG. 5. (Color online) Crystal truncation rods 11L and 22L of sample A and the model of the epitaxial film used in the calculations. The film contains 23 full layers of Fe_3Si and an additional FeSi atomic layer at the surface, thus starting and ending with the FeSi layers. Two top FeSi layers are disordered with respect to positions of Fe and Si atoms (order parameter β=0.5). The experimental data are shown by open circles and the calculations by red lines. The insets magnify the vicinities of the Bragg reflections 111 and 222.

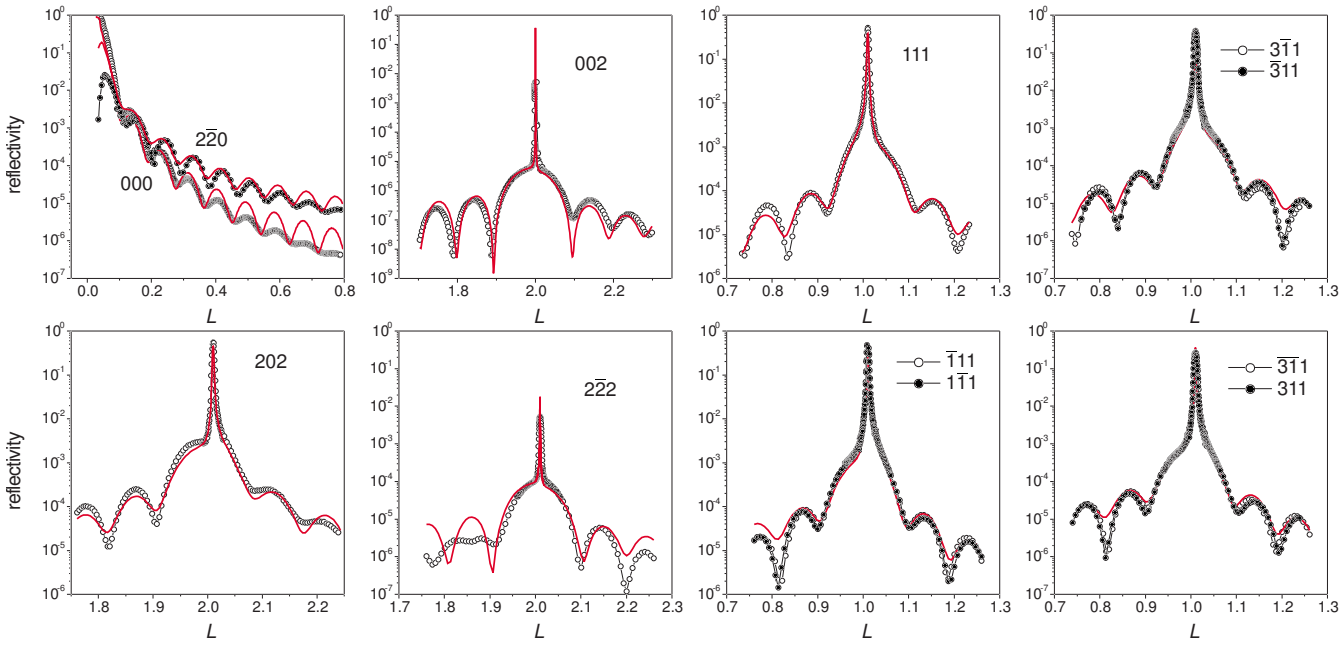

FIG. 6. (Color online) Measured and calculated crystal truncation rods of sample B. The experimental data are shown by open and full circles and the calculations by red lines. Thickness of Fe_3Si film is 22 ML.

since the measured 222 reflection is about five times broader (and accordingly less intense) than the calculated dynamical peak from the quasiforbidden GaAs reflection. The agreement in the intensities along the whole CTR, obtained after this scaling, proves the consistency of the approach. The agreement of the experimental and calculated 11*L* rods is less crucial, since the width of the measured 111 reflection from the GaAs substrate is close to the theoretical value.

A comparison of the measured and calculated curves shows that structure A (Fig. 3) is realized in this sample. Hence, the Fe_3Si layer begins with the FeSi atomic layer at the interface. An important feature of the experimental curves is the presence of pronounced thickness oscillations in the whole range of *L*, in particular, in the middle between the Bragg reflections. These oscillations are evidence of the perfect thickness uniformity of the film. A change of the film thickness by just 1 ML would add one more oscillation to the range between the Bragg peaks, so that oscillations in the middle between the Bragg peaks were in antiphase with respect to each other. Any average, either coherent (if the terraces were smaller than the coherence length) or incoherent (if the terraces were larger), would blur the oscillations. Hence, the film thickness within the active surface area is constant, with an accuracy better than 1 ML. The width of the active surface area is defined by the slits (0.7 mm) before the sample. Its length is limited by the detector slits (2×2 mm^2) as well as the varying angular position of the detector, as it follows the rod. As a result, the active surface area has a width of 0.7 mm and a length of typically 3–4 mm. An exception is the CTR 111 for $L \lesssim 1$, where a length up to 7 mm is reached. Since thickness oscillations are blurred only for the CTR 111 and only at *L* smaller than 1 [see Fig. 5(a)], we conclude that the film thickness is uniform (with the accuracy of 1 ML) within about 5 mm along the sample.

The film thickness can be obtained directly from the period ΔL of the thickness intensity oscillations as $N = 2/\Delta L$. Using this formula, we obtain $N = 24$ from the 11*L* rod. However, the intensity fringes are not uniform along the 22*L* rod: we find the same thickness of 24 ML from the fringes in the vicinity of the 220 reflection but the vicinity of the 222 reflection gives $N = 23$. The discrepancy is clearly visible when the calculation of the 22*L* rod is performed for 24 full ML (not shown here): the oscillations in the measured and the calculated curves are in phase near the 220 reflection and antiphase close to 222. The agreement is notably improved when the top Fe layer is removed: the film model contains 23 full ML and an additional FeSi layer on the top, as shown in Fig. 5(c). This is in accordance with other studies[40–44] which show that the surface of a Fe_3Si crystal is silicon rich. The measured intensity oscillations along the 11*L* rod show beats, marked by the arrows in Fig. 5(a). Similar beats can be reproduced in the calculations by assuming that the top two FeSi layers are disordered in the Fe and Si sublattices ($\beta = 0.5$), so that the top layers have the B2 structure. This correction of the model also improves the agreement in the positions of the intensity maxima close to the 111 reflection [shown in the inset of Fig. 5(a)]. A disorder at the interface does not give rise to such beats. That allows us to distinguish between the disorder at the surface and at the interface.

Figure 6 presents a set of measured and calculated CTRs for sample B. Several equivalent reflections, obtained by a 180° rotation of the sample, were measured to check for systematic errors. The corresponding curves (shown on top of each other with open and filled circles on the plots) coincide, thus proving the absence of a sample miscut or misalignment. Since sample B begins with a Fe layer at the interface (see Fig. 2), it ends with the FeSi atomic layer at the surface, after an integer number of monolayers. A simultaneous fit of all CTRs, shown in Fig. 6, is reached by as-

suming almost complete lack of long-range order in the top FeSi layer (α=0.15 and β=0.5) and additional disorder within the second FeSi layer (β=0.5). The 202 reflection is fairly sensitive to the relaxation (shift in the [001] direction) of the whole Fe_3Si film. We find a relaxation of $0.04a$ =0.22 Å toward the substrate. Other reflections are less sensitive to the relaxation. The CTRs near the 000 (the reflectivity curve) and 220 reflections of sample B show a damping of the thickness oscillations away from the Bragg peaks. This damping originates from a nonuniform film thickness. Its analysis is outside the scope of the present paper.

V. CONCLUSIONS

We have performed MBE growth of Fe_3Si films on GaAs(001) and studied their order and structure *in situ* by measuring the x-ray crystal truncation rods. We calculate the intensity distribution along the whole CTR, including the dynamical diffraction peaks, and use the dynamical peaks to set the measured peaks on an absolute scale. The films are fully ordered in the Fe and Si sublattices, with the exception of 1 or 2 ML at the surface. These top monolayers are disordered, predominantly within the FeSi atomic layer. We find two types of interfacial structures, with the first film layer on top of the last As layer of the GaAs substrate containing either only Fe atoms or both Fe and Si atoms. In both cases, the Si atoms in the first FeSi layer are located in between the top Ga-As atomic chains. We speculate that the choice of the interfacial structure depends on the residual arsenic at the surface. The films end with the FeSi layer at the surface, irrespective of the type of the interface. A Fe_3Si film relaxation of 0.22 Å toward the substrate is found.

ACKNOWLEDGMENTS

The authors thank Jens Herfort for fruitful discussions, and Claudia Herrmann, Steffen Behnke, Hans-Peter Schönherr, Brad Tinkham, and Tatsuro Watahiki for support during the experiments.

[1] C. J. Palmstrøm, Annu. Rev. Mater. Sci. **25**, 389 (1995).
[2] G. A. Prince, Science **282**, 1660 (1998).
[3] J. Herfort, H.-P. Schönherr, and K. H. Ploog, Appl. Phys. Lett. **83**, 3912 (2003).
[4] J. Herfort, H.-P. Schönherr, K.-J. Friedland, and K. H. Ploog, J. Vac. Sci. Technol. B **22**, 2073 (2004).
[5] J. Herfort, B. Jenichen, V. Kaganer, A. Trampert, H.-P. Schönherr, and K. H. Ploog, Physica E (Amsterdam) **32**, 371 (2006).
[6] J. Herfort, A. Trampert, and K. H. Ploog, Int. J. Mater. Res. **97**, 1026 (2006).
[7] I. K. Robinson, Phys. Rev. B **33**, 3830 (1986).
[8] I. K. Robinson, R. T. Tung, and R. Feidenhans'l, Phys. Rev. B **38**, 3632 (1988).
[9] C. A. Lucas and D. Loretto, Appl. Phys. Lett. **60**, 2071 (1992).
[10] C. A. Lucas, G. C. L. Wong, and D. Loretto, Phys. Rev. Lett. **70**, 1826 (1993).
[11] C. A. Lucas, D. Loretto, and G. C. L. Wong, Phys. Rev. B **50**, 14340 (1994).
[12] J. Harada, Y. Itoh, T. Shimura, I. Takahashi, J. C. Alvarez, and N. S. Sokolov, Appl. Surf. Sci. **75**, 263 (1994).
[13] H. Hashizume, M. Sugiyama, T. Niwa, O. Sakata, and P. L. Cowan, Rev. Sci. Instrum. **63**, 1142 (1992).
[14] T. Niwa, M. Sugiyama, T. Nakahata, O. Sakata, and H. Hashizume, Surf. Sci. **282**, 342 (1993).
[15] D. Bahr, J. Falta, G. Materlik, B. H. Müller, and M. Horn-von Hoegen, Physica B **221**, 96 (1996).
[16] J. Falta, D. Bahr, G. Materlik, B. H. Müller, and M. Horn-von Hoegen, Surf. Rev. Lett. **5**, 145 (1998).
[17] I. K. Robinson, P. O. Nilsson, D. Debowska-Nilsson, W. X. Ni, and G. V. Hansson, Appl. Phys. Lett. **79**, 2913 (2001).
[18] G. Renaud, A. Barbier, and O. Robach, Phys. Rev. B **60**, 5872 (1999).
[19] M. Tabuchi, R. Takahashi, M. Araki, K. Hirayama, N. Futakuchi, Y. Shimogaki, Y. Nakano, and Y. Takeda, Appl. Surf. Sci. **159-160**, 250 (2000).
[20] Y. Takeda and M. Tabuchi, J. Cryst. Growth **237-239**, 330 (2002).
[21] M. Tabuchi and Y. Takeda, J. Cryst. Growth **298**, 12 (2007).
[22] R. Feidenhans'l, Surf. Sci. Rep. **10**, 105 (1989).
[23] I. K. Robinson and D. J. Tweet, Rep. Prog. Phys. **55**, 599 (1992).
[24] U. Pietsch, V. Holý, and T. Baumbach, *High-Resolution X-Ray Scattering: From Thin Films to Lateral Nanostructures* (Springer, Berlin, 2004).
[25] B. Jenichen, V. M. Kaganer, J. Herfort, D. K. Satapathy, H. P. Schönherr, W. Braun, and K. H. Ploog, Phys. Rev. B **72**, 075329 (2005).
[26] A. M. Afanas'ev, P. A. Aleksandrov, S. S. Fanchenko, V. A. Chaplanov, and S. S. Yakimov, Acta Crystallogr., Sect. A: Found. Crystallogr. **42**, 116 (1986).
[27] R. Colella, Phys. Rev. B **43**, 13827 (1991).
[28] A. Caticha, Phys. Rev. B **47**, 76 (1993).
[29] A. Caticha, Phys. Rev. B **49**, 33 (1994).
[30] T. Takahashi and S. Natakani, Surf. Sci. **326**, 347 (1995).
[31] T.-S. Gau and S.-L. Chang, Acta Crystallogr., Sect. A: Found. Crystallogr. **51**, 920 (1995).
[32] O. Litzman and P. Mikulik, J. Phys.: Condens. Matter **11**, 5767 (1999).
[33] V. Holý and P. F. Fewster, J. Phys. D **36**, A5 (2003).
[34] S. G. Podorov, N. N. Faleev, K. M. Pavlov, D. M. Paganin, S. A. Stepanov, and E. Förster, J. Appl. Crystallogr. **39**, 652 (2006).
[35] K. M. Pavlov, D. M. Paganin, D. J. Vine, and L. Kirste, Phys. Status Solidi A **204**, 2613 (2007).
[36] V. M. Kaganer, Phys. Rev. B **75**, 245425 (2007).
[37] B. Jenichen, W. Braun, V. M. Kaganer, A. G. Shtukenberg, L. Däweritz, C.-G. Schulz, K. H. Ploog, and A. Erko, Rev. Sci. Instrum. **74**, 1267 (2003).
[38] B. Jenichen, V. M. Kaganer, W. Braun, J. Herfort, R. Shayduk, and K. H. Ploog, Thin Solid Films **515**, 5611 (2007).
[39] E. Vlieg, J. Appl. Crystallogr. **30**, 532 (1997).
[40] H. Busse, J. Kandler, B. Eltester, K. Wandelt, G. R. Castro, J. J. Hinarejos, P. Segovia, J. Chrost, E. G. Michel, and R. Miranda,

Surf. Sci. **381**, 133 (1997).
[41] U. Starke, W. Meier, C. Rath, J. Schardt, W. Weiß, and K. Heinz, Surf. Sci. **377-379**, 539 (1997).
[42] U. Starke, J. Schardt, W. Weiss, W. Meier, C. Polop, P. L. de Andres, and K. Heinz, Europhys. Lett. **56**, 822 (2001).
[43] M. Vondráček, V. Dudr, N. Tsud, P. Lejček, V. Cháb, K. C. Prince, V. Matolín, and O. Schneeweiss, Surf. Sci. **600**, 4108 (2006).
[44] J. Hafner and D. Spišák, Phys. Rev. B **75**, 195411 (2007).